Superalloys 2008
Roger C. Reed, Kenneth A. Green, Pierre Caron, Timothy P. Gabb, Michael G. Fahrmann, Eric S. Huron and Shiela A. Woodard
TMS (The Minerals, Metals & Materials Society), 2008

GRAIN BOUNDARY AND INTRAGRANULAR DEFORMATIONS DURING HIGH TEMPERATURE CREEP OF A PM NICKEL-BASED SUPERALLOY

A. Soula[1], Y. Renollet[1], D. Boivin[1], J.-.L. Pouchou[1], D. Locq[1], P. Caron[1], Y. Bréchet[2]

[1]Office National d'Études et de Recherches Aérospatiales (ONERA), BP 72, F-92322 Châtillon Cedex, France
[2]Laboratoire de Thermodynamique et de Physico-Chimie Métallurgiques (LTPCM), INPG,
Domaine Universitaire, BP 75, F-38402 St Martin d'Hères Cedex, France

Keywords: Disk Superalloy, Powder Metallurgy, Microstructure, Mechanical Properties

Abstract

Grain boundary and intragranular deformations have been analysed during high temperature creep of a PM nickel-based superalloy. Local deformation has been quantified using an original microextensometry technique. This technique consists in calculating deformation of ceramic square grids deposited on flat specimens thanks to an electron lithography technique. Grain boundary sliding (GBS) was quantified by measuring microgrid offsets at grain boundaries. Strain maps and GBS maps have been computed. Superimposition with electron back scattered diffraction (EBSD) maps allowed studying the influence of grain boundary character on their deformation behaviour. The effectiveness of this technique was demonstrated through creep test performed at 700, 750 and 800°C under an applied stress of 700 MPa. The results showed that grain boundary and intragranular mechanisms of deformation accommodate one's each other to preserve the continuity of deformation in the material. Modification of deformation mechanisms within grains was related to coarsening of tertiary γ' precipitates with increase of temperature. Simultaneously, decrease of GBS contribution was observed when temperature increases.

Introduction

Gas turbine engine performances are highly dependent on the capacity of high-pressure disk materials to withstand intermediate-temperature/high-stress exposures for several thousands of hours. High-strength fine-grained nickel-based superalloys processed by the powder metallurgy (PM) route are thus currently used for high-pressure turbine disk applications in military and civil aeroengines. The PM superalloys NR3 and NR6 were developed to satisfy the requirements for disk applications with improved creep strength and thermal stability at temperatures above 650°C [1]. Up today, the analysis of the creep behaviour of the alloy NR3 has been mainly focused on the effect of microstructural parameters, such as grain size and distribution of strengthening γ' precipitates [2, 3]. Special attention has been paid to intragranular deformation mechanisms operating during creep tests at high temperature and under a wide range of applied stresses. The results of these studies suggest that grain boundary sliding (GBS) could play a key role as a deformation process [3].

The aim of the present work is to study grain boundary and intragranular mechanisms of deformation using a microgrid technique during the creep behaviour at high temperature of a PM superalloy. Local strain maps and grain boundary sliding maps will be computed. Contribution of GBS to macroscopic strain will be evaluated. Relationships between the grain boundary characteristics and their deformation behaviour will then be analysed.

Material

NR6 alloy is a superalloy developed at ONERA for high temperature disk applications [3, 4]. Its chemistry (Table I) was designed in order to avoid the precipitation of topologically close-packed (TCP) phase particles which can occur during long-term exposures at high temperatures and to increase the suitability for supersolvus solutioning. The total volume fraction of strengthening γ' phase was estimated to be within the 0.40-0.45 range. The γ' solvus and solidus temperatures of NR6 were measured to be respectively 1175°C and 1230°C. The density of this alloy is 8.22 g.cm^{-3}.

Table I. NR6 Alloy Composition (wt.%)

Ni	**Co**	**Cr**	**Mo**	**W**	**Al**	**Ti**
Bal.	14.8	14.0	2.0	4.1	3.1	4.5
Hf	**B**	**C**	**Zr**			
0.33	0.012	0.023	0.053			

The NR6 alloy was processed by Aubert & Duval and Snecma using the following PM route: vacuum induction melting, argon atomisation, powder sieving ($\phi \leq 75$ µm (-200 mesh)), hot compaction, hot extrusion and isothermal forging. All the thermomechanical operations were conducted below the γ' solvus temperature.

Samples were taken from a single as-forged pancake. A supersolvus heat treatment was applied in order to obtain a coarse-grained microstructure which usually exhibits better creep properties than fine-grained material at temperature equal to or greater than 700°C [3]. All the samples of this study were heat treated as follows: 1190°C/2h [100°C/min cooling rate] + 700°C/24h [air cooling (AC)] + 800°C/4h [AC]. The resulting microstructure was examined using optical (OM) and scanning electron microscopy (SEM) techniques (Figure 1 and Figure 2). The mean grain size and the mean secondary γ' precipitate size were measured to be respectively 26 µm and 225 nm. Fine tertiary γ' precipitates (10 to 40 nm) were also observed in the γ matrix channels (Figure 2).

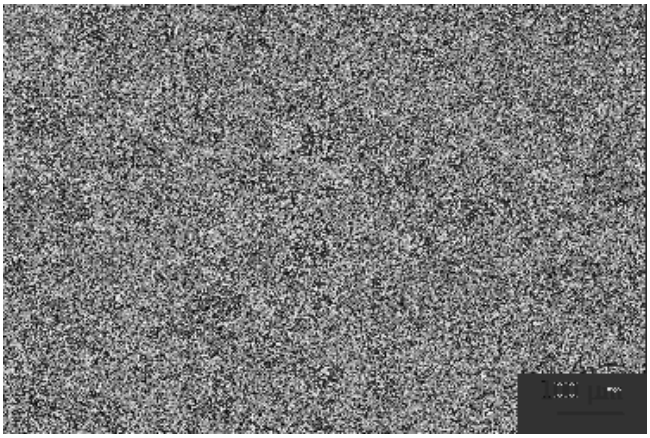

Figure 1. OM micrograph of NR6 microstructure after the supersolvus heat treatment (grain size).

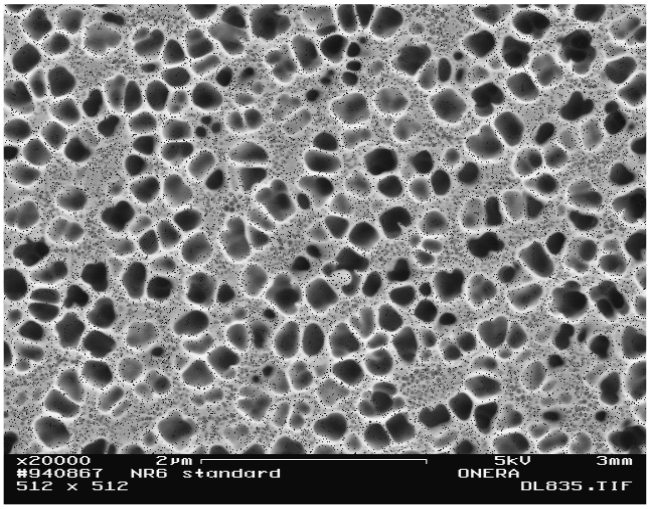

Figure 2. SEM micrograph of NR6 microstructure after the supersolvus heat treatment (secondary and tertiary γ' precipitates).

Creep Tests

Constant load creep tests were performed in tension on flat specimens (section: 4.2 x 2.5 mm^2, gauge length: 31 mm). Creep tests were conducted in high-vacuum (~ 10^{-4} Pa) to avoid significant oxidation of the superalloy which could restrict the image analysis procedure quality. Creep tests performed at 700, 750 and 800°C and 700 MPa and were also interrupted at strain levels of 0.2, 0.5 and 1%.

Microextensometry

The microextensometry technique consists of: i) depositing grids on the creep specimen, ii) measuring grid displacements and, iii) computing the deformation field of the grids.

High Temperature Microgrids

Square grids were deposited at the centre of the widest face of the creep specimen after careful mechanical polishing (1/4 µm diamond) and using an electron lithographic technique. The stages of this technique are: i) coating of the specimen surface with polymethyl methacrylate (PMMA) resist, ii) irradiation of the resist by an electron beam in a scanning electron microscope (SEM), iii) developing (dissolution of the irradiated resin), iv) depositing of the grid material by pulverization and, v) non irradiated resist stripping by chemical dissolution. More data about the technique are detailed in [5]. Meticulous control of the different scanning settings and of the resist deposit, chemical dissolution and pulverization parameters is absolutely necessary to obtain high quality microgrids.

Considering the mean grain size and the scanning settings, 318 x 318 μm^2 microgrids were made in order to cover at least 150 grains. Similarly, the pitch and the width line of the microgrids are respectively 5 µm and 0.5 µm so as to obtain several grid line intersections along one grain boundary and several unit cells in one grain (Figure 4).

Gold or platinum microgrids are usually chosen for room or intermediate temperature (up to 500°C) experiments [6, 7, 8]. Unfortunately, microgrid technique is seldom used for high temperature micromechanical studies because of thermal instability of the grid [9]. Now, for this study, high stability of the microgrid was needed to get high quality SEM images. Several refractory materials were tested as grid material and hafnia (HfO_2) was lastly selected. This material meets the following criteria: i) high thermal stability, ii) good deformability: the grid material must follow the superalloy deformation and, iii) significant chemical contrast between the superalloy and the grid for high quality SEM images using back scattered electron emission.

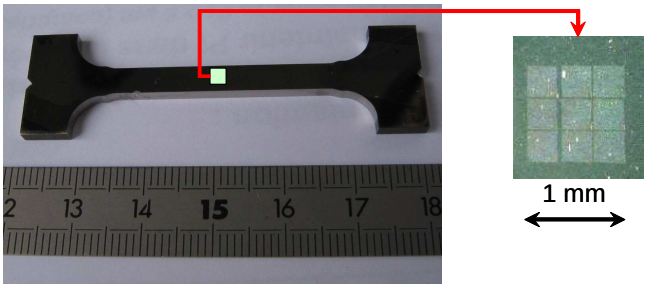

Figure 3. Flat specimen for creep test.

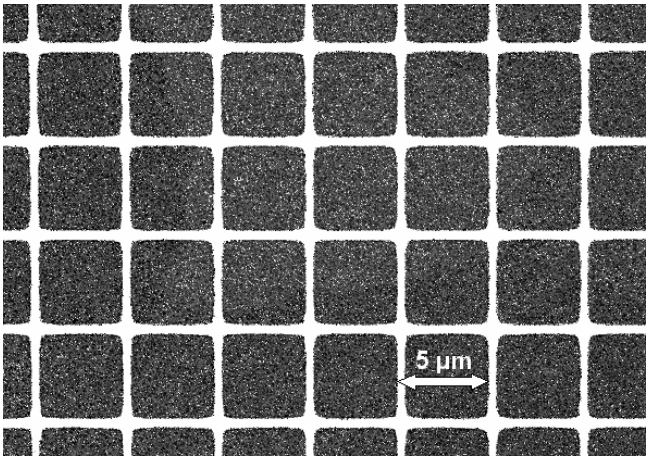

Figure 4. SEM micrograph of a microgrid.

Deformation calculation

Classic digital image correlation is based upon the grey level distribution of specific objects on images (for example, the grid nodes: intersections of vertical and horizontal lines of the grid). This implies that this distribution must be retained after creep deformation. Unfortunately, this condition is not achieved in our experiments because local deformation or slight superalloy oxidation induce local grey level distribution changes. So, a specific image analysis procedure was developed and applied to the grids in order to quantify in-plane displacement field.

High resolution SEM images of the grid (8000 x 8000 pixels) were recorded before and after deformation. A cross-like grid node pattern was defined for each image. This pattern was correlated with all the nodes of the grid in the image (Figure 5). This correlation procedure provided the coordinates (x, y) of each node. The respective node coordinates in the undeformed and deformed state gave the in-plane displacement field D defined as follows for each node:

$$D = \begin{pmatrix} u_x(x,y) \\ u_y(x,y) \end{pmatrix} \quad (1)$$

where $u_x(x, y)$ and $u_y(x, y)$ are the components of the displacement vector along the x and y axes for the node of coordinates (x, y).

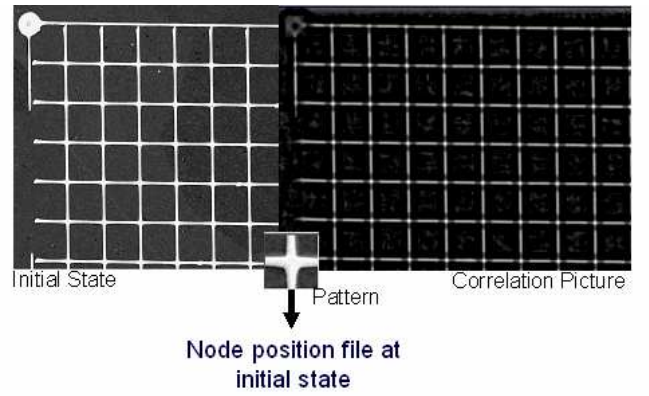

Figure 5. Correlation procedure using a cross-like grid node pattern to obtain the coordinates of each node.

Derivation of the displacement field at each node gives the deformation field. Hence, at each node the tensor of deformation E is calculated. In small deformation theory, the Green-Lagrange tensor E can be approximated to ε as follows:

$$\varepsilon = \frac{1}{2}\begin{pmatrix} 2\dfrac{\partial u_x(x,y)}{\partial x} & \dfrac{\partial u_x(x,y)}{\partial y} + \dfrac{\partial u_y(x,y)}{\partial x} \\ \dfrac{\partial u_x(x,y)}{\partial y} + \dfrac{\partial u_y(x,y)}{\partial x} & 2\dfrac{\partial u_y(x,y)}{\partial y} \end{pmatrix} \quad (2)$$

The three deformation components at the node (x, y) are then computed according to the following equations:

$$\varepsilon_{xx}(x,y) = \frac{u_x((x-\Delta x),y) - u_x((x+\Delta x),y)}{|2\Delta x|} \quad (3)$$

$$\varepsilon_{yy}(x,y) = \frac{u_y(x,(y-\Delta y)) - u_y(x,(y+\Delta y))}{|2\Delta y|} \quad (4)$$

$$\varepsilon_{xy}(x,y) = \frac{1}{2}\left(\frac{u_x(x,(y-\Delta y)) - u_x(x,(y+\Delta y))}{|2\Delta y|} + \frac{u_y((x-\Delta x),y) - u_y((x+\Delta x),y)}{|2\Delta x|} \right) \quad (5)$$

where Δx and Δy are the distances between the grid points in x and y directions (Figure 6).

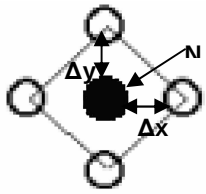

Figure 6. Integration field when deformation tensor is computed at a node N (black solid circle). The open circles represent the neighbouring nodes used for the calculation.

Intergranular Deformation Calculation.

Strain maps do not allow direct quantification of GBS. Calculated deformation at nodes on both sides of a grain boundary underestimates the GBS deformation value. Indeed, use of calculated deformation at neighbouring nodes is equivalent to affecting a grain boundary thickness related to the integration field width (10µm in our study). So a specific treatment was developed to estimate grain boundary deformation.

GBS between two grains leads to the occurrence of offsets along vertical or horizontal lines of the grid. GBS is characterized by a sliding vector **S** (Figure 7). GBS deformation can be quantified by the measurements of *u* and *w* at each point where grid line discontinuities are observed [10].

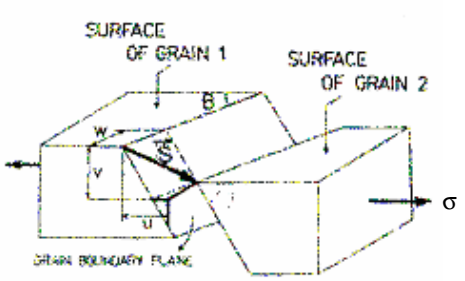

Figure 7. Sliding vector **S** between two adjacent grains 1 and 2: *u, v, w* are the three sliding offsets, θ the angle between the trace of the boundary on the surface and the tensile axis [10].

In order to perform a full statistical analysis of grain boundary sliding on grid, the sliding vector **S** is estimated at each intersection of a grid line with grain boundaries. The vector is calculated as follows:

$$\mathbf{S = D_{n+1} - D_n} \quad (6)$$

where D_{n+1} and D_n are the displacement vectors at nodes located on both sides of a grain boundary.

Sliding strain along the tensile axis is given by:

$$\varepsilon_{GBS} = \frac{\overline{u}}{d} \quad (7)$$

where d is the average grain size, $\overline{u}$ is the average value of u obtained from projection of **S** along the tensile axis.

The contribution of GBS to the total strain is then expressed as:

$$\xi = \frac{\varepsilon_{GBS}}{\varepsilon_t} \quad (8)$$

where ε_t is the total strain (average of the computed strains ε_{xx} on the grid, axis x being the tensile axis).

Grain Boundary Characterization

Electron back scattered diffraction (EBSD) measurements were performed on grid areas by orientation mapping of undeformed creep specimen in a Zeiss DSM 960 SEM equipped with the OIM™ software from TSL. Grain boundaries (GB) were categorized according to the coincidence site lattice (CSL) model and the Brandon's criterion [11]. In particular, Σ3 GB were defined as twin boundaries, $3 < \Sigma \leq 29$ GB as special boundaries and $\Sigma > 29$ GB as general (random) boundaries. Proportion of grain boundary class on a grid defined as previously is given in Table II. Additionally, custom software ANAGRA developed at ONERA provided in a single data file, morphological information as grain boundary length, distribution and orientation to tensile axis as well as the grain boundary character.

Table II: Grain Boundary Character Distribution in NR6 Alloy

GB category	Σ3	$3 < \Sigma \leq 29$	$\Sigma > 29$
Number fraction (%)	40.9	10.6	48.5

EBSD maps were obtained with sample tilted at 70° for optimum diffraction conditions while microgrid SEM images were recorded at 0° tilt. In order to accurately superimpose the EBSD maps on grid images, another custom algorithm was developed. Once this superimposition achieved, it is possible to overlay EBSD map on deformation field map or GBS amplitude map.

Results

As expected, use of high temperature microgrids allows evidencing localised deformation events. After interrupted creep tests, grid line discontinuities are observed at grain boundaries but also at intersections between grid lines and intragranular slip bands (ISB). Such typical examples are illustrated in Figure 8. ISB's are interpreted as resulting from high activity of plastic deformation in narrow bands, as observed for instance during tensile deformation of single crystal superalloys [12]. Such bands were also observed in PM nickel-base superalloys [13, 14, 15] during creep at 650 and 700°C under high stress.

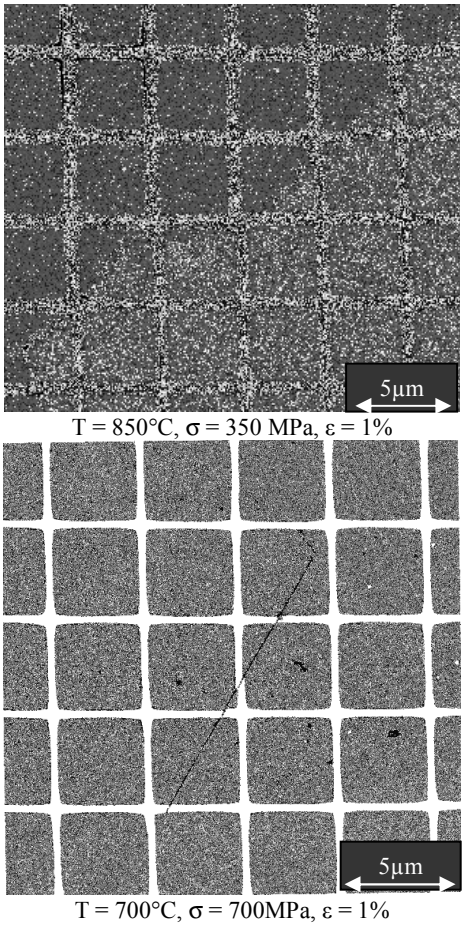

T = 850°C, σ = 350 MPa, ε = 1%

T = 700°C, σ = 700MPa, ε = 1%

Figure 8. Deformation events observed during creep tests, SEM micrographs (BSE).

Attempts to quantify the local strain after only 0.2% and 0.5% of creep deformation failed because the local displacement fields are too small. Indeed, the correlation procedure does not allow measurement of displacement field below 1 pixel (40 nm). Quantification of local strain was thus only possible after 1% of creep deformation.

However, qualitative analysis can be performed after a creep deformation less than 1%. Grid lines discontinuities are indeed detectable with one's own eyes at grain boundaries and at slip lines after only 0.2 or 0.5% of creep deformation, even if the quantification of deformation is impossible. Such a qualitative analysis was performed for instance to determine the effect of temperature and creep strain on the percentage of grains where slip bands are observed.

At a given temperature, the number of grains exhibiting ISB increases with the creep strain (Figure 10). For example, at 700°C and at 0.2% of creep strain, ISB's are observed in only 1.2% of the grains whereas at 1% of creep strain, 16% of grains were concerned by ISB. When the creep temperature increases, the percentage of grains exhibiting ISB decreases. At 0.5% of creep strain, when temperature reaches 800°C, no slip activity within

grains is observed whereas at 700°C, slip activity concerns about 7% of the grains.

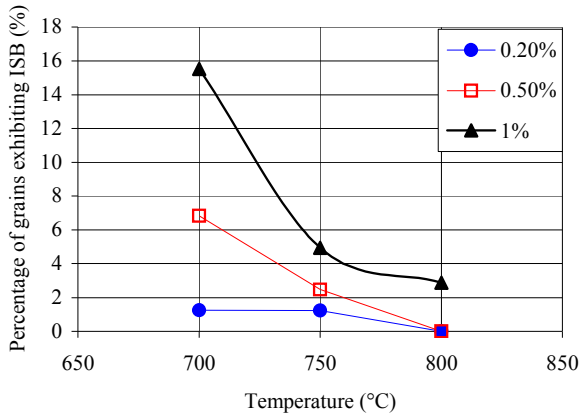

Figure 9. Influence of temperature and strain on the percentage of grains exhibiting ISB (σ = 700MPa).

Moreover, the microextensometry technique allows calculating strain maps and thus provides precious information about the distribution of the deformation at the grain scale and at the grid area scale. As an example, at 700°C in some grains the deformation is not distributed homogeneously, but concentrated in areas where slip bands are observed or in the neighbourhood of grain boundaries (Figure 10). Intragranular deformation can thus vary from 0.5% to 4% within a given grain. In grains where there is no slip activity, deformation is homogeneous and is about 0.5%. At 750 and 800°C, maximal deformations measured on the grid are smaller than at 700°C. Moreover, highest values are located at grain boundaries and intragranular deformation is distributed homogeneously within the grains. At 800°C, local intragranular deformation is about 1%.

The degree of heterogeneity of the deformation can be characterized by the standard deviation of the grid average strain (normalized by the grid average strain). In agreement with the former observations, increasing temperature leads to smaller standard deviation values. Standard deviation is 0.69 at 700°C, 0.57 at 750°C and 0.51 at 800°C (Figure 11).

As intergranular deformation is concerned, analysis of GBS amplitude maps (GBS amplitude is defined as the **S** amplitude) after a creep deformation of 1% reveals that GBS mean amplitude is lower at 800°C than at 700°C. Furthermore, maximal GBS amplitude is observed at grain boundaries oriented at 30 to 60° from the tensile axis. Superimposition of GBS maps to EBSD maps showed that all boundaries have an ability to glide (Figure 12). GBS occurs at some twin boundaries. Those grain boundaries are generally located at 45° to the tensile axis, orientation for which the resolved stress is maximal. In order to
In addition, the contribution of GBS to the total strain can be calculated after each creep test. Figure 11 shows that when temperature increases (and so creep rate), the contribution of GBS to the total strain decreases.

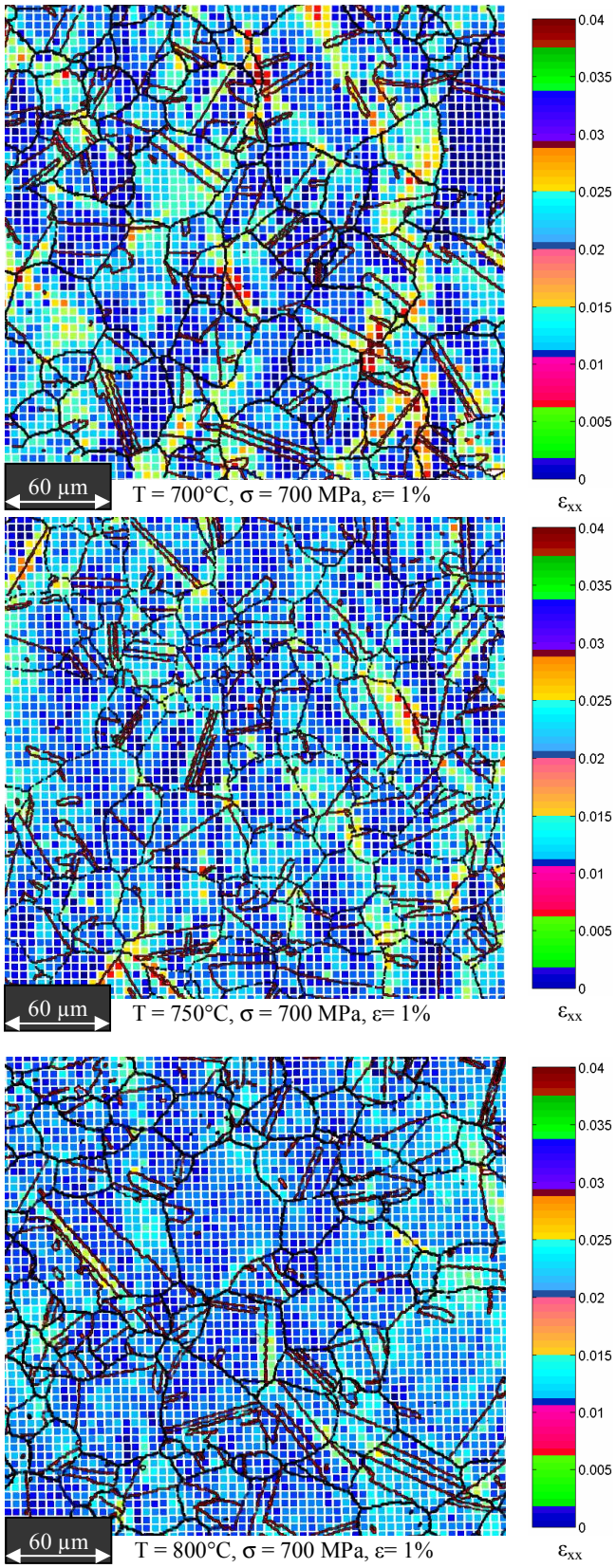

Figure 10. Distribution of the deformation after creep at 700, 750 and 800°C, superimposition of strain maps and of EBSD maps.

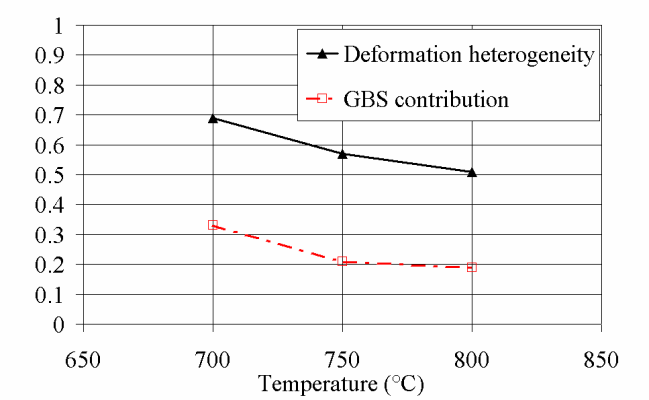

Figure 11. Influence of temperature on deformation heterogeneity and on the contribution of GBS to creep strain (ε_t = 1%, σ = 700 MPa).

Discussion

Increasing temperature leads to changes in the distribution of the deformation within the material and in the respective contributions of intergranular and intragranular slip mechanisms. When the temperature increases, intragranular slip activity decreases and the strain is distributed more homogeneously within the grains.

Recent works of Locq et al. [3] on NR3 and Unocic et al. [13] on René 88DT and René 104 have highlighted the influence of γ' precipitates size on the creep mechanisms at 650 and 700°C. These PM superalloys exhibit γ/γ' microstructures comparable to that of NR6. Thanks to TEM observations, a change in deformation mechanism was evidenced when dissolution of tertiary γ' precipitates occurred. In unaged samples, shearing of γ' particles occurred by <112>{111} slip leaving stacking faults in extended deformation bands in NR3 and by microtwinning in René 88DT and René 104. When tertiary γ' precipitates are dissolved, both authors observed a/2 <110> matrix dislocations bypassing the secondary γ' particles by a combined glide/climb mechanism. Indeed at 700°C, it was noticed in NR3 alloy that the coarsening of the tertiary γ' precipitates is very sluggish [14]:

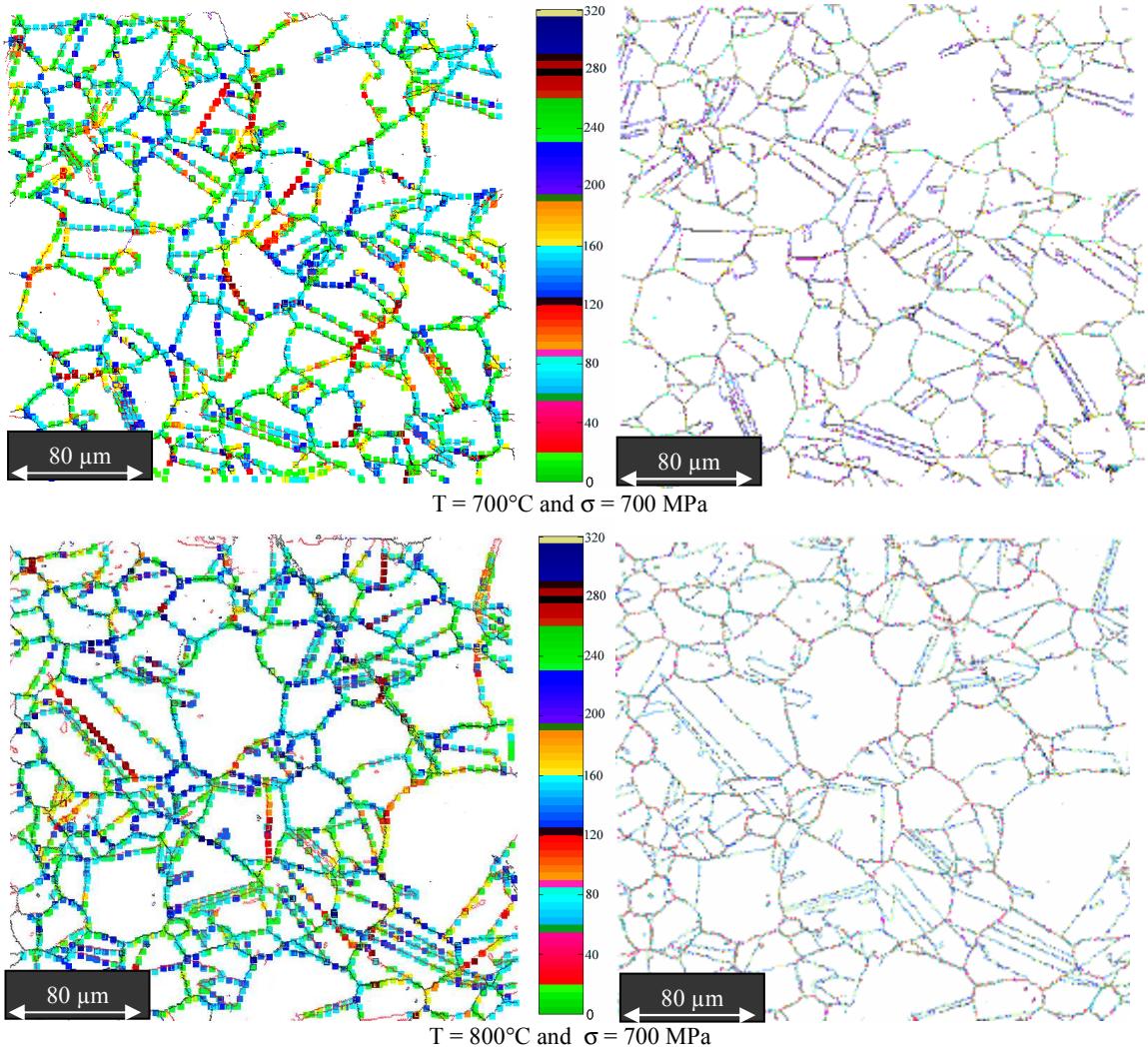

Figure 12. GBS amplitude maps at 700°C and 800°C (unit = nm) and EBSD maps (red: twin boundaries, black: random boundaries, blue: special boundaries) after creep at 700°C and 800°C.

large quantities of tertiary precipitates were observed by TEM after ageing at 700°C during 1000 and 5000 hours. These durations greatly exceeded the time necessary to get to 1% of creep strain at 700°C and 700 MPa (typically 200 hours for NR6 alloy). When increasing creep temperature, tertiary γ' precipitates first coalesce and lastly are dissolved. At 800°C, Wlodek [16] showed that there is no more γ' precipitates in N18 after about 10 hours. So, it is assumed that during creep test (including dwell time at 800°C and the creep test time to reach 1%), only few (or no more) of these precipitates remain in NR6. We can thus infer that during creep of NR6 at 800°C, intragranular deformation operates mainly by a glide and climb by-pass mechanism of the secondary γ' precipitates as observed in overaged NR3, René 88DT and René 104 superalloys. That explains the homogenization of the intragranular deformation and the decrease of the number of ISB events within the grains when the temperature increases.

GBS can be considered as a deformation process or as an accommodation process of deformation in polycrystals [17]. In other words, grains may suffer plastic deformation to accommodate sliding at grain boundaries or GBS may occur to compensate the incompatibility of deformation at the interface between two grains. The present results are consistent with both theories that makes difficult to determine which mechanism is first activated. At low temperature, creep deformation is difficult and located in slip bands because of the presence of fine tertiary γ' precipitates and GBS amplitude is high. At high temperature, creep deformation within grain is more homogeneous within grains because of the absence of the fine tertiary γ' precipitates and GBS amplitude is lower. If we compare two grains without any ISB after creep at 700°C and at 800°C, the mean strain value is higher at 800°C. This last observation is consistent with the decrease of the contribution of GBS when temperature increases. Particularly, according to equations 9 and 10 [18], GBS decrease must be balanced by an increase of intragranular deformation.

$$\varepsilon_t = \varepsilon_G + \varepsilon_{GBS} \quad (9)$$

$$\varepsilon_G = \varepsilon_t \left(1 - \frac{\varepsilon_{GBS}}{\varepsilon_t}\right) \quad (10)$$

This analysis supports the fact that GBS activity and intragranular activity are linked processes. Intragranular deformation and grain boundary sliding accommodate one's each other to preserve the continuity of deformation in the material. The way of accommodating will change with respect to temperature. This change is linked with microstructure evolution occurring in NR6 superalloy when temperature increases.

Conclusion

Microgrids developed for microextensometry have been used to detect and quantify intragranular and intergranular deformations. A specific process based on image analysis was developed to obtain local strain field and GBS amplitude maps. Information about grain boundary characteristics and orientation to tensile axis obtained by EBSD were superimposed to those maps.

Creep tests were performed under a tensile stress of 700MPa at 700, 750 and 800°C. Microextensometry technique was shown to be very efficient to reveal local deformation. Qualitative (at low 0.2% and 0.5% creep strain) and quantitative analysis (at 1% creep strain) were performed. These analyses confirmed that intragranular mechanisms of deformation are related tertiary γ' precipitates distribution and size. Furthermore, it has been established that GBS contribute to high temperature creep deformation of PM nickel-based superalloys. This contribution is highly linked with mechanism of deformation activated within grains.

These promising results confirm the efficiency of the microextensometry technique developed to investigate the role of GBS in high temperature creep of superalloys. Further investigations are in progress, using the same approach, to study the influence of strain and stress on local deformation mechanisms.

References

1. D. Locq, M. Marty, A. Walder, and P. Caron, "Development of new PM superalloys for high temperature applications," *Intermetallics and Superalloys, EUROMAT*, Vol. 10, ed. D.G. Morris, S. Naka and P. Caron (Weinheim, Germany: WILEY-VCH Verlag Gmbh, 2000), 52-57.

2. D. Locq, M. Marty, and P. Caron, "Optimisation of the mechanical properties of a new PM superalloy for disk application," *Superalloys 2000*, ed. T.M. Pollock et al. (Warrendale, PA: TMS, 2000), 395-403.

3. D. Locq, P. Caron, S. Raujol, F. Pettinari-Sturmel, A. Coujou, and N. Clément, "On the role of tertiary γ' precipitates in the creep behaviour at 700°C of a PM disk superalloy," *Superalloys 2004*, ed. K.A. Green et al. (Warrendale, PA: TMS, 2004), 179-187.

4. C. Duquesne et al., "Nickel-based superalloys with high temperature stability," US Patent #5,815,792, 1996.

5 M.A. McCord and M.J. Rooks., *Handbook of microlithography, micromachining and microfabrication* (Bellingham, WA: SPIE Press, 1997).

6. A. Karimi., "Plastic low study using the microgrid technique," *Mat. Sci. Eng.*, 63 (1984), 267-276.

7. R.A. Carolan et al., "The effect of grain boundary deformation on the creep micro-deformation of copper," *Acta Met. Mat.*, 40 (1992), 1629-1636.

8. E. Héripré et al., “Coupling between experimental measurements and polycrystal finite element calculations for micromechanical study of metallic materials,” *Int. J. of Plasticity*, 23 (9) (2007), 1512-1539.

9. X. Carbonneau et al., “Development of high temperature extensometric microgrids,” *J. Mat. Sci. Letters*, 16 (1997), 1101-1103.

10. R.L. Bell et al., “The contribution of grain boundary sliding to the overall strain of a polycristal,” *Trans. Met. Soc. AIME*, 11 (1967), 1821-1823.

11. D.G. Brandon, “The structure of high-angle grain boundaries,” *Acta Met.*, 14 (1966), 1479-1484.

12. P. Caron and T. Khan, “Tensile Behaviour of a Nickel-Based Single Crystal Superalloy: Effects of Temperature and Orientation,” *Proceedings of the First ASM Europe Technical Conference on Advanced Materials and Processing Techniques for Structural Applications*, ed. T. Khan and A. Lasalmonie (Châtillon, France: ONERA, 1987), 59-70.

13 R.R. Unocic, G.B. Viswanathan, P.M. Sarosi, S. Karthikeyan, J. Li, M.J. Mills, “Mechanisms of creep deformation in polycrystalline Ni-Base disk superalloys,” *Mat. Sci. Eng. A*, 483–484 (2008), 25–32.

14 S. Raujol, “Influence du vieillissement sur le comportement en fluage d’un superalliage pour disques de turbine” (Ph.D. thesis, Institut National des Sciences Appliquées de Toulouse, 2004).

15 R. Couturier, H. Burlet, S. Terzi, S. Dubiez, L. Guetaz, and G. Raisson, “Process development and mechanical properties of alloy U720LI of high temperature turbine disks,” *Superalloys 2004*, ed. K.A. Green et al. (Warrendale, PA: TMS, 2004), 351-359.

16 S. T. Wlodek, M. Kelly, D. Alden, “The structure of N18,” *Superalloys 1992*, ed. S.D. Antolovich et al. (Warrendale, PA : TMS, 1992), 467-476.

17 T.G. Langdon, “Grain boundary sliding revisited: developments in sliding over four decades,” *J. Mater. Sci*, 41 (2006), 597-609.

18 J.D. Parker, B. Wilshire, “A surface measurement study of grain boundary sliding during creep of a two phase, Copper-Cobalt Alloy,” *Mater. Sci. Eng.*, 29 (1977), 219-225.